A Quality Consensus Strategy for Binarization of Neuronal Images

A thesis

submitted in partial fulfilment of the requirement for the Degree of

Master of Computer Application

of

Jadavpur University

By

Dipannita Banerjee

Registration No.: **149868 of 2019-20**

Examination Roll No.: **MCA226005**

Under the Guidance of

Dr. Subhadip Basu

Department of Computer Science and Engineering

Jadavpur University, Kolkata-700032

India

2022

FACULTY OF ENGINEERING AND TECHNOLOGY

JADAVPUR UNIVERSITY

Certificate of Recommendation

This is to certify that the dissertation entitled **"A Quality Consensus Strategy for Binarization of Neuronal Images"** has been carried out by **Dipannita Banerjee** (University Registration No.: **149868 of 2019-20**, Examination Roll No.: **MCA226005**) under my guidance and supervision and be accepted in partial fulfilment of the requirement for the Degree of Master of Computer Application. The research results presented in the thesis have not been included in any other paper submitted for the award of any degree in any other University or Institute.

……

Dr. Subhadip Basu (Thesis Supervisor)

Department of Computer Science and Engineering

Jadavpur University, Kolkata-32

Countersigned

…….

Prof. Anupam Sinha

Head, Department of Computer Science and Engineering,

Jadavpur University, Kolkata-32.

…….

Prof. Chandan Majumdar

Dean, Faculty of Engineering and Technology,

Jadavpur University, Kolkata-32.

FACULTY OF ENGINEERING AND TECHNOLOGY

JADAVPUR UNIVERSITY

CERTIFICATE OF APPROVAL*

This is to certify that the thesis entitled **"A Quality Consensus Strategy for Binarization of Neuronal Images"** is a bonafied record of work carried out by **Dipannita Banerjee** in partial fulfillment of the requirements for the award of the degree of Master of Computer Application in the Department of Computer Science and Engineering, Jadavpur University during the period of September 2019 to July 2022. It is understood that by this approval the undersigned does not necessarily endorse or approve any statement made, opinion expressed, or conclusion drawn therein but approves the thesis only for the purpose for which it has been submitted.

……..

Signature of Examiner 1

Date:

……..

Signature of Examiner 2

Date:

*Only in case the thesis is approved

FACULTY OF ENGINEERING AND TECHNOLOGY

JADAVPUR UNIVERSITY

Declaration of Originality and Compliance of Academic Ethics

I hereby declare that this thesis entitled "A Quality Consensus Strategy for Binarization of Neuronal Images" contains a literature survey and original research work by the undersigned candidate, as part of her degree in Master of Computer Application.

All information has been obtained and presented in accordance with academic rules and ethical conduct.

I also declare that, as required by these rules and conduct, I have fully cited and referenced all materials and results that are not original to this work.

Name: Dipannita Banerjee

Registration No: 149868 of 2019-20

Exam Roll No.: MCA226005

Thesis Title: A Quality Consensus Strategy for Binarization of Neuronal Images

…..……..

Signature with Date

ACKNOWLEDGEMENT

I would like to start by thanking the holy trinity for helping me deploy all the right resources and for shaping me into a better human being. I would like to express my deepest gratitude to my advisor, **Dr. Subhadip Basu**, Department of Computer Science and Engineering, Jadavpur University for his admirable guidance, care, patience, and for providing me with an excellent atmosphere for doing research. Our numerous scientific discussions and his many constructive comments have greatly improved this work.

This project is partially supported by the CMATER research laboratory of the Computer Science and Engineering Department, Jadavpur University, India. Words cannot express my indebtedness to **Prof. Mahantapas Kundu,** Department of Computer Science and Engineering, Jadavpur University for his amazing guidance and supervision. I am deeply grateful to **Prof. Mita Nasipuri**, for the long discussions that helped to enrich the technical content of this manuscript. I would like to thank **Prof. Ram Sarkar**, Department of Computer Science and Engineering, Jadavpur University, for helping me to deal with the problem related to image binarization.

I would like to thank **Dr. Jakub Wlodarczyk,** Department of Molecular and Cellular Neurobiology, Nencki Institute of Experimental Biology, Warsaw, Poland for providing the essential data for our research without which we can't test our method's efficiency.

Among the seniors, I am deeply grateful to **Mr. Nirmal Das** for his guidance and supervision throughout the project work. Without his enthusiasm, encouragement, support, and continuous optimism this thesis would hardly have been continued. I would like to thank **Mr. Neelotpal Chakraborty** for educating me about Mendeley, which has proved to be an indispensable tool to site research papers and providing the template for this thesis.

I am also thankful to my friends **Mr. Subhrabesh Dutta and Ms. Soumee Mukherjee** who were always present to motivate me.

Most importantly none of this would have been possible without the love and support of my family. I extend my thanks to my parents, especially to my mother whose forbearance and whole-hearted support helped this endeavour succeed.

This thesis would not have been completed without the inspiration and support of a number of wonderful individuals — my thanks and appreciation to all of them for being part of this journey and making this thesis possible.

……..

Dipannita Banerjee

Registration No: 149868 of 2019-20

Examination Roll No.: MCA226005

Department of Computer Science & Engineering

Jadavpur University

ABSTRACT

In the field of neural processing, the dendritic spines are likely to be of major importance. The morphology of dendritic spines is very diverse and changes in spine size, as well as their density, are thought to reflect changes in the strength of the synaptic transmission. This paper presents a modified image binarization technique for the neuronal image. Binarization is often recognized to be one of the most important steps in most high-level image analysis systems, particularly for object recognition. It's precise functioning highly determines the performance of the entire system. Although so much research work has been done so far in the field of image binarization still there is a scope for improvement. All of those methods perform well to some extent but in every case, there are a lot of disconnected spines, deformities in dendritic shape and size, and a lot of manual work needs to be done. Image binarization is the process of converting a greyscale image to a black and white image. This image binarization technique is used as a pre-processing step of image analysis in various domains. Thresholding is a method that is used for binarization. In thresholding, an optimal threshold value is chosen and the pixels are classified as foreground or background by comparison with this threshold value. In this paper, we have used local thresholding. Locally adaptive image binarization with a sliding-window threshold can be an effective tool for various image processing tasks. The major focus of this thesis report is to provide a new technique for binarization of medical images using the classical method of Sauvola with some modifications. The experiment deals with the quality consensus that is if one of the decisions for a particular pixel says to be foreground and the other says to be background then foreground is taken of all the variable window sizes and the precision of the neuronal image is evaluated.

CONTENTS

LIST OF FIGURES

LIST OF TABLES

CHAPTER 1: INTRODUCTION

The major goal behind studying and analyzing the medical image is to offer a huge potential to contribute to the advancement of medical treatment. Almost all the medical image processing techniques[1] need to produce a binary form of the original image and it plays an essential role in many medical image segmentation[2] techniques. Locally adaptive image binarization with a sliding window [3] threshold can be an effective tool for various image processing tasks. The advantages[4] of obtaining first a binary image are that it reduces the complexity of the data and simplifies the process of image segmentation**.** The threshold is one of the most powerful techniques for image segmentation[5]. The medical image [6] is converted to a binary image using the threshold value. Thresholding creates a binary image from grayscale images by turning all pixels[7] below the threshold to zero representing the background and all pixels about that threshold to one for foreground representation[8]. Finding the correct threshold value is a challenging process. Because of its efficiency in performance and its simplicity, thresholding techniques have been studied extensively and a large number of thresholding methods have been developed[9].

1.1 BINARIZATION AND THRESHOLDING

*Binarization***:** Image Binarization[10] is the technique of changing any grayscale photo right into a binary photo (Black & White photo). Grayscale images and Binary images are two important variations among digital images. In a grayscale image, a particular pixel takes an intensity value lying between 0 to 255 whereas in a binary image it could take only two values either 0 or 255. Therefore, only 1 bit is sufficient to represent one pixel. Image Binarization aims to segment the foreground text from the document background. A fast and accurate image binarization technique is important for the ensuing image processing tasks [11].

Binarization is the pre-processing step for image analysis and processing[12]. Binary images are used to represent basic shapes and line drawings. Binarization techniques are used to simplify the image.

Thresholding: Thresholding is one of the old, simple, and popular techniques for image segmentation. Thresholding can be done based on global information or it can be done using local information of the image [13].

The simplest thresholding methods replace each pixel in an image with a black pixel if the image intensity $I_{i,j}$ is less than some fixed constant T (that is, $I_{i,j} < T$), or a white pixel if the image intensity is greater than that constant[14].

Binarization technique can be grouped into two categories: Global and Local. Global binarization methods pick one threshold value for the entire document images which is often based on an estimation of the background level from the intensity histogram of the image. These methods are very fast and produce good results. These methods fail when there are nonuniform illuminated document images. The local (adaptive) binarization method uses different values for each pixel according to the local area information[15].In most methods, the same threshold is applied to all the pixels of an image. However, in some cases, it can be advantageous to apply a different threshold to different parts of the image, based on the local information of the pixels. This category of methods is called local or adaptive thresholding[16]–[18]. In those cases, a user-defined neighborhood is defined and a threshold is computed for each pixel and its neighbourhood. Many global thresholding methods can be adapted to work locally, but there are also methods developed specifically for local thresholding.

1.2 BINARIZATION WITH RESPECT TO BIOMEDICAL IMAGES

Medical image-breaking technologies[2] now offer a huge potential to contribute to the advancement of healthcare and medicine. Image-guided approaches have expanded to incorporate not just diagnostic but also therapeutic procedures. Healthcare is becoming increasingly reliant on information, research, networking, picture archiving and distribution, equipment, and treatment based on physical energies, in addition to traditional image viewing and analysis[19].

Binarization plays a crucial role in gaining a complete comprehension of image information. Segmented pictures are now frequently employed in a variety of applications, including diagnosis, treatment planning, pathology localization, anatomical structure investigation, and computer-integrated surgery. Particularly, medical images are often corrupted by noise and sampling artefacts, which can cause considerable difficulties when applying rigid methods[20].

1.3 NEURONAL AND DENDRITIC SPINE IMAGES

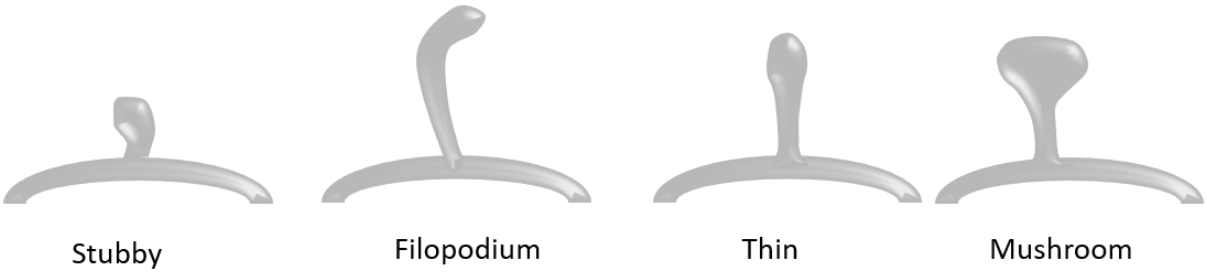

Figure 1: Different Spine Morphologies

Dendritic spines are morphological specializations that protrude from the main shaft of neuronal dendrites. Typically, 0.5–2 μm in length (but up to 6 μm in the CA3 region of the hippocampus)[21][22], dendritic spines are found at a linear density of 1–10 spines per μm of dendritic length in mature neurons[23]. Dendritic spines are actin-rich small protrusions on dendritic branches where most of the excitatory synapses are localized. During the spinogenesis process as the spine started to develop, they build a long thin thread-like form, called a filopodium.[24] Filopodium is usually witnessed during development. This type of spine has a long neck and no head. Over time filopodia is replaced by a thin i.e., spine with a long neck and small head, stubby i.e. spines with no neck or short neck, and relatively mature mushroom-shaped spines i.e. spines with a long neck and large bulbous head.[25] Spine morphology and stabilization are highly influenced by synaptic activity. Mushroom-shaped spines, consider to be mature spines are typically more stable and have an enlarged spine head containing neurotransmitter receptors and a postsynaptic density (PSD). In contrast, filopodium is an immature spine with a lack of synapses.[26]

It is used in controlling electrical and biochemical compartmentalization and plays a significant role in activity and signal transmission in neural networks [27]**.** The shape of dendritic spines changes either spontaneously, or in response to generated neuronal stimulation [28] [29]. These changes are related to learning, memory [30], and various neurodegenerative and neuropsychiatric diseases [31],[32]**,**[33]e.g., Alzheimer's disease [34]**,** schizophrenia [35]. Many aspects of the existing structure-function relationship in dendritic spines are still unknown due to their complex morphology and plasticity [30]**,** [33]. It should be emphasized that variability in spine shapes is expressed through a continuous spectrum, and therefore the use of the arbitrary classification of type is a simplification [36]. However, it is assumed that the strength of synaptic connections

correlates with the morphological features of spines, their turnover, or both. Therefore, for example, mushroom spines are known as mature spines that can create stable synaptic connections, while thin spines represent immature forms usually named learning spines, due to their high potential for plastic changes (for details see [37][38] Apart from mushroom and thin spines, there are also other distinguishable classes, such as stubby, filopodium, cup-shaped and spine-head protrusions, which also reveal specific electrophysiological properties of synapses located on the aforementioned spines [39]**,** [40]**.** Spines may also undergo pathological plasticity in which transformations between immature to mature forms are disturbed. Thus, the knowledge of underlying structural plasticity in physiology is extremely important to understanding how the brain functions in pathological conditions **(**[37]**;** [41]). Due to the small size (up to a dozen μm) of dendritic spines, and also the limitations related to microscopic imaging, the accurate structural analysis of spine morphometry remains a challenge.

The goal behind studying and analyzing the dendritic spine is to offer a huge potential to contribute to the advancement of medical treatment. Ketamine is an N-methyl-D-aspartate receptor antagonist that has gained wide attention as a potent antidepressant. It has also been recently reported to have prophylactic effects in animal models of depression and anxiety. Alterations of neuroplasticity in different brain regions; such as the hippocampus; prefrontal cortex; and amygdala; are a hallmark of stress-related disorders; and such changes may endure beyond the treatment of symptoms. The present study investigated whether a prophylactic injection of ketamine has effects on structural plasticity in the brain in mice that are subjected to chronic unpredictable stress followed by an 8-day recovery period. Ketamine administration (3 mg/kg body weight) 1 h before stress exposure increased the number of resilient animals immediately after the cessation of stress exposure and positively influenced the recovery of susceptible animals to hedonic deficits. At the end of the recovery period; ketamine-treated animals exhibited significant differences in dendritic spine density and dendritic spine morphology in brain regions associated with depression compared with saline-treated animals. These results confirm previous findings of the prophylactic effects of ketamine and provide further evidence of an association between the antidepressant-like effect of ketamine and alterations of structural plasticity in the brain[32]

1.4 MOTIVATION

In the last few decades, so much research work has been done so far in the field of image binarization still there is a scope for improvement. All of those methods perform well to some extent but in every case, there are a lot of disconnected spines, deformities in dendritic shape and size, and a lot of manual work needs to be done. Most of the existing methods involve some serious manual intervention which needs a lot of time and effort from the researchers to binarize a single image. Therefore, we need to develop an automatic method that minimizes user intervention and also gives the desired result with better precision.

1.5 OBJECTIVE

The major focus of this thesis report is to provide a new technique for binarization of medical images using the classical method of Sauvola with some modifications. Sauvola's method[42] used a local adaptive threshold for a fixed size of the window where a threshold is determined for each pixel based on statistics computed from a local window centered on the pixel of interest. In our proposed experiment we have taken variable window sizes. For each window, the pixel decision is taken whether the pixel is foreground or background, and based on the decision the consensus value is taken into consideration. The experiment deals with the quality (if one of the decisions for a particular pixel says to be foreground and the other says to be background then foreground is taken) consensus of all the variable window sizes and the precision of the neuronal image is evaluated. The experiment then is compared with the other classical method.

1.6 ORGANIZATION OF THE THESIS

In *Chapter 1*, we have discussed the basic introduction of binarization. A brief introduction to the utilization of binarization in the medical image. We have also discussed the neuronal images and dendritic spines and their importance in various areas of medical experiments.

In *Chapter 2*, a brief survey of different work that has been done so far to binarize the dendritic spine's shape and nature has been presented, and from this is how we get our motivation for work.

In *Chapter 3*, the proposed methodology that has been adopted is explained along with the appropriate algorithm. We selected the method described by Sauvola as our reference binarization method.

In *Chapter 4*, Several datasets for binarization of degraded neuronal images with ground truth pixel labelling have been proposed and used for evaluation in the literature. The primary way that binarization algorithms are currently evaluated is by comparison to reference ground truth (GT) binarizations.

In *Chapter 5*, The comparison results and experimental output images are then discussed with the success stories of the proposed methodology and also the error case.

In *Chapter 6*, an overall discussion of the work related to its advantage, shortcomings, and future scopes are also discussed and concluded.

CHAPTER 2: SURVEY

2.1 OTSU'S METHOD

Otsu method[43] is a global thresholding method that converts grayscale images into bi-level images. This technique divides the pixels into two classes one is foreground and the other is background. It chooses an optimal threshold that separates the image into two different classes. The threshold value is chosen such that the within-class variance is minimized and the between-class variance is maximized. The algorithm exhaustively searches for the threshold that minimizes the intra-class variance, defined as a weighted sum of variances of the two classes:

$$\sigma_{\omega}^2(t) = \omega_0(t)\sigma_0^2(t) + \omega_1(t)\sigma_1^2(t)$$

where weights $\omega_0(t)$ and $\omega_1(t)$ are the probabilities of the two classes separated by a threshold t and σ_0^2 and σ_1^2 are variances of these two classes.

Otsu method gives its best performance for only those images that have a clear bi-modal pattern. But neuronal and dendritic images normally don't have such a clear-cut pattern. Besides this, it does not perform well for images with uneven illumination and shadow.

2.2 NIBLACK'S METHOD

Niblack's method [44] is a local thresholding method. In local thresholding methods, a different threshold value is calculated for each pixel. It uses local statistics of the image, such as variance, and range to calculate the threshold. In the Niblack method, a rectangular window is a slide over the grayscale image to estimate the threshold of the pixels. It uses the local statistics mean and standard deviation of the window to estimate the threshold. Threshold T(i,j) is estimated as shown in the below equation

$$T(i,j) = \mu + k \times \sigma$$

Where μ represents the mean of the window and σ represents the standard deviation of the window. The value of k is a constant and it defines the size and quality of binarization. As this method is dependent upon the local features of the image, it gets affected by blank areas in the image and is also not efficient for the images with background noise.

2.3 SAUVOLA'S METHOD

The Sauvola method[42] is the improvement of the Niblack method. It is a local variance method that uses standard deviation. The threshold is calculated as shown in the equation:

$$T(i,j) = \mu\left[1 + k\left(\frac{\sigma}{R} - 1\right)\right]$$

In the above equation, μ is the mean and σ is the standard deviation of the window. Values suggested for k and R are 0.5 and 128. The window size and value of k will affect the quality of the image but R will have very little effect. This method is used for images having uneven illumination, light texture, and stained images. But Sauvola method thins the image after its application.

2.4 BERNSEN METHOD

Bernsen's method [45]uses the contrast of the image. Then threshold is estimated as the average of the highest and lowest intensity values in the window. The below equation calculates the local contrast of the window.

$$c(i,j) = I_{max} - I_{min}$$

The pixels are categorized as foreground or background by comparing the local contrast with a threshold value. The pixel will be classified as background if the local contrast is found to be less than the threshold and vice-versa. Bernsen's method doesn't perform well for the images having more complex backgrounds.

2.5 LOCAL MAXIMA AND MINIMA

This method[46] uses contrast which depends upon the local minimum and maximum. A normalization factor is introduced which will compensate for the effect of variation in the image background. Image contrast is calculated as shown in the below equation:

$$c(i,j) = \frac{I_{max} - I_{min}}{I_{max} + I_{min} + \epsilon}$$

High contrast image pixels are found from the contrast image. Then local thresholding is performed with a threshold value calculated from the found high contrast image pixels. It is not suitable for the bright text with a proper bright background.

CHAPTER 3: METHODOLOGY

In this section, the proposed algorithm for binarization is explained. We have implemented a simple and effective method for neuronal image binarization in the presence of various degradations of the dendritic spine.

3.1 PROPOSED METHOD

Here we have tried to improve 'Sauvola's Method'[42] as it was recommended[10] for binarizing images having uneven illumination, light texture, and stained images. By original Sauvola's method, there are two parameters named k and R and their recommended values are k=0.5 and R=128. But applying these values to neuronal and dendritic images we did not get the desired result. By experimenting and after lots of trial and error we decided to use k=0.1 and R=90.

After overcoming the issue of setting the correct value of this k and R, we gave attention to the precision of the output images with respect to the prepared ground truth. For this, we use the n-star quality consensus method, which means we are taking various window sizes (from 5 to 17) and applying the improved Sauvola's Method to each window and taking a decision from these based on whether at least 1 window to all 7 windows say that the particular pixel is white or black.

3.2 ALGORITHM

The algorithm, for applying our proposed method, is as follows –

Step 1. Start the method by taking an image as grayscale. Let $\boldsymbol{img}[\boldsymbol{i},\boldsymbol{j}]$ be the matrix representation of the input grayscale image and $\boldsymbol{dx}$ and $\boldsymbol{dy}$ be the height and width of that image.

Step 2. For each pixel $[\boldsymbol{i},\boldsymbol{j}]$ we select the window from **5×5** to **17×17** respectively and for each window, we calculate the mean and standard deviation. Then we calculate the threshold value of that particular window by using the following Eq. 6-

$$\boldsymbol{T(i,j) = \mu\left[1 + k\left(\frac{\sigma}{R} - 1\right)\right]} \qquad \boldsymbol{Eq.1}$$

where, $\boldsymbol{\mu = mean,\ \sigma = standard\ deviation, k = 0.1,\ R = 90}$

Step 3. We compare the threshold value with the pixel value as follows-

If $\boldsymbol{img}[\boldsymbol{i},\boldsymbol{j}] < \boldsymbol{T}[\boldsymbol{i},\boldsymbol{j}]$ then **return** black otherwise, white.

Step 4. We count, whether the pixel is black or white for each window from **5×5** to **17×17** and store the count value for that pixel.

Step 5. Now we are deciding between each pixel if any one of the windows says that the pixel is white (if $\boldsymbol{white\ count} >= \boldsymbol{1}$), then $\boldsymbol{img}[\boldsymbol{i},\boldsymbol{j}]$ is white otherwise black. Similarly, we decide on at least 2 white counts for all the 7 white counts respectively.

Step 6. Then we apply the filter to all those 7 raw images. The filter is for removing all the background white noises by inspecting whether that pixel is surrounded by 8 or 7 or 6 black pixels. Then we apply the morphological close operation on those filtered images by choosing a **3×3** window.

Step 7. Now save the output images.

CHAPTER 4: INPUT DATA DESCRIPTION & GROUND TRUTH PREPARATION

This study[41] was carried out in accordance with the Ethical Committee on Animal Research of the Nencki Institute, based on the Polish Act on Animal Welfare and other national laws that are in full agreement with the EU directive on animal experimentation. All effort was made to minimize animal suffering. Dissociated hippocampal cultures from postnatal day 0 Wistar rats were prepared as described below[48].

Brains were removed and hippocampi were isolated on ice in dissociation medium DM; 81.8 mM Na2SO4, 30 mM K2SO4, 5.8mM MgCl2, 0.25 mM CaCl2, 1 mM HEPES pH 7.4, 20 mM glucose; 1mM kynurenic acid; 0.001% Phenol Red. Next, hippocampi were incubated twice for 15 minutes at 37ºC with 100 units of papain (Worthington, NY) in DM, then rinsed three times in DM and subsequently three times in plating medium [MEM, 10% fetal bovine serum (FBS) and 1% penicilin-streptomycin]. Hippocampi were triturated in a plating medium, then centrifuged for 10 minutes at room temperature, at 208.5 g. The resulting cell pellet was suspended in a plating medium, cells were counted and plated at a density of 120,000 cells per 18-mm-diameter coverslip (Assistant, Germany) coated with 1 mg/ml poly-L-lysine (Sigma) and 2.5 μg/ml laminin (Roche). At 3 hours after plating medium was exchanged for maintenance medium (Neurobasal-A without Phenol Red, 2% B-27 supplement, 1% penicillin-streptomycin, 0.5 mM glutamine, 12.5μM glutamate, 25μM β-mercaptoethanol) and cells were kept at 37°C, under a humidified 5% CO2 atmosphere. Cultured hippocampal neurons were transfected for 14 days in vitro (DIV) with Syn-GFP plasmid to visualize neuronal morphology. Live-cell imaging was performed on 20–22 DIV. Prior to the imaging, the cells were placed in an acquisition chamber with a controlled temperature (37 ºC) and stable CO2 (5%) concentration Dendritic segments that were decorated with dendritic spines were imaged at time 0, before stimulation, and then cLTP was induced by bath application of a mixture of 50μM forskolin, 50μM picrotoxin, and 0.1μM rolipram (each dissolved in dimethylsulfoxide [DMSO]) in maintenance media. Dendritic segments were imaged 10 min and 40 min after cLTP induction. Images were acquired using a Carl Zeiss LSM780 confocal microscope with a C-Apochromat 40×/1.2 NA water immersion objective using a 488 nm wavelength argon laser at 3% transmission and 70 nm/pixel resolution. A series of z-stacks were acquired at 0.2 μm steps. Nine different neurons from rat dissociated

hippocampal cultures were imaged using a confocal light microscope, before and after chemically induced long-term potentiation (cLTP). All the images were captured twice, one at baseline (before cLTP stimulation) and the other after 10 minutes from cLTP induction. During image preprocessing, we took maximum intensity projection(MIP) of the confocal z-stack and perform Gaussian de-noising on the 2-D MIP image. The preprocessed MIP images at time 0 are labeled as T0 and the images captured after 10 minutes are labeled as T10. In this experiment, total of 459 dendritic spines are manually segmented and annotated by experimental biologists in both T0 and T10 images using an open-source image analysis software, Fiji [49] and ITKSnap[50].

In the first dataset, three different neurons from rat dissociated hippocampal cultures were imaged using a confocal light microscope, before and after cLTP induction. All of the images were captured three times: at baseline (before cLTP) and 10 and 40 min after cLTP induction. In the second dataset, three different neurons from rat dissociated hippocampal cultures were similarly imaged at baseline and 10 and 40 min after mock cLTP induction (i.e., only the solvent, DMSO, was used). During image pre-processing, we took the confocal z-stack and performed Gaussian de-noising on the 3-D image stack. The pre-processed images at time 0 are labelled as T0, and the images that were captured at 10 and 40 min are labeled as T10 and T40, respectively. The preparation of the brain slices was based on [51]. For the visualization of changes in the shape of dendritic spines, 1,1′-Dioctadecyl-3,3,3′,3′-Tetramethylindocarbocyanine Perchlorate (DiI) staining in stressed and control mice was performed. The mice were anesthetized and the trans cardinal perfusion with 1,5% paraformaldehyde was performed. Then the brains were dissected and sliced using a vibratome. Slices (140μm thick) that contained the different brain structures recovered for at least 1.5 h at RT. Random dendrite labelling was performed using 1.6μm tungsten particles (Bio-Rad, Hercules, CA, USA) coated with a propelled lipophilic fluorescent dye (DiI; Invitrogen) that were delivered to the cells by gene gun (Bio-Rad) bombardment. Images of dendrites were acquired under 561 nm fluorescent illumination using a confocal microscope (63×objective, 1.4NA) at a pixel resolution of 1024 × 1024 with a 3.43 zoom, resulting in a 0.07μm pixel size. A series of z-stacks were acquired at 0.2μm steps.

For *Ground Truth* preparation, we use Microsoft Paint. By putting the input grayscale image and a rough binarized version of that input grayscale image (obtained by applying normal Sauvola's method) side by side, we observed this pixel by pixel and correct the rough binarized image manually so that it can be used as a ground truth. While creating the ground truth we have taken care of all the disconnected spines, any sort of shape deformities, background noises, any unwanted lone pixels, etc.

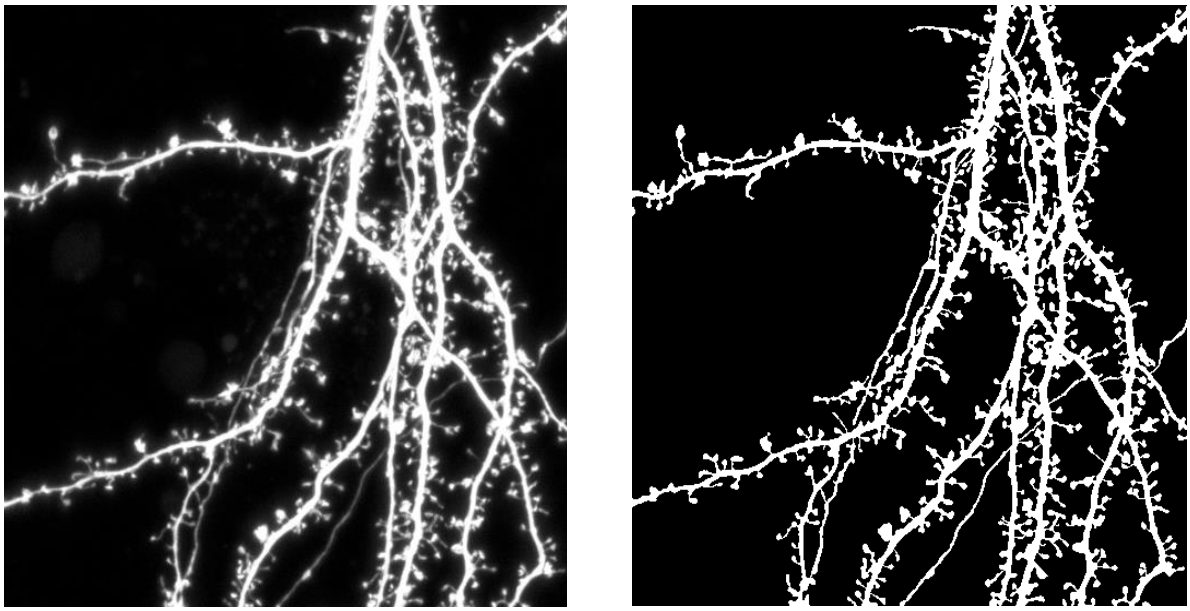

(a) (b)

Figure 2 A dendritic spine image (a) Grayscale image of the dendritic spine (b) ground truth of the same image prepared using Microsoft paint

CHAPTER 5: RESULTS

After applying our method to these input images, we compare our result to the prepared ground truth. Here we use three parameters to judge our result, the metrics that are suitable for the comparison of the performance of different binarization algorithms are F-measure, Recall, and Precision respectively.

5.1 PRECISION

Precision is true pixels extracted divided by total pixels extracted[52]. Precision is given as shown in the below equation:

$$Precision = \frac{TP}{TP + FP}$$

TP denotes true positive i.e. the pixels that are foreground in both ground truth and binarized image. FP denotes false positive i.e. pixels identified as foreground in the binarized image but are actually background in the ground truth image.

5.2 RECALL

Recall is the true pixels extracted divided by the total number of true pixels[53]. Recall is given as shown in the below equation:

$$Recall = \frac{TP}{TP + FN}$$

TP denotes true positive i.e. the pixels that are foreground in both ground truth and binarized image. FN denotes false-negative i.e. the pixels identified as background in the binarized image but are actually foreground in the ground truth image.

5.3 F- MEASURE

F-Measure is given as shown in the below equation:

$$F - Measure = \frac{2 \times Precision \times Recall}{(Precision + Recall)}$$

F-Measure is the harmonic mean of Precision and Recall. Its value should be high for better results.

5.4 EXPERIMENTAL IMAGES & TABLE OF RESULTS

The result of the different algorithms is included for comparison in this section. Here we are including all the input and output images obtained through the various known method as well as through our proposed method along with the table of comparison of F-Measure, Recall, and Precision for quantitative evaluation [54].

5.4.1 COMPARISON OF THE DATASET WITH OTSU, NIBLACK, SAUVOLA, AND THE PROPOSED METHOD

5.4.1.1 First Data sample0_1 (1024×1024)

We first take one of the 1024×1024 images (Fig: 2(a)) collected as mentioned in the data description chapter previously. Then we apply Otsu's method, Niblack's method, and Sauvola's method (Here in the figure we have shown a window size of 11 but for the experiment we have taken windows of variable sizes ranging from 5 to 17, the result is shown in the below table) and our proposed algorithm (Here in the figure we have shown quality consensus for at least 7 pixels but for the experiment, we have shown all consensus data) on the same image respectively.

In the proposed algorithm we have also applied the noise filter to get rid of unwanted lone white pixels from the output image.

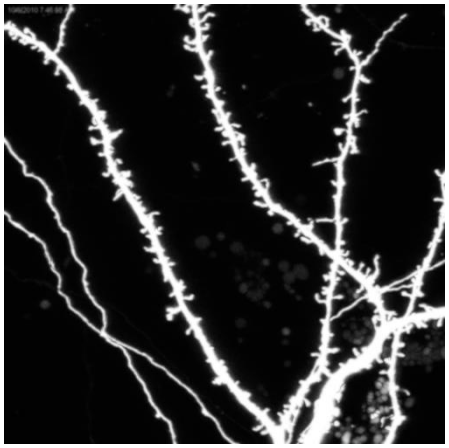

(a)

(d)

(b)

(e)

(c)

(f)

Figure 3: sample0_1 (a) Input Grayscale Image, (b) Prepared Ground Truth, (c) Otsu's Method, (d) Niblack's Method, (e) Sauvola's Method with Window Size =11 (f) Sauvola Ensemble (Quality consensus- at least 7)

After storing all the outputs, we calculated the quality comparison parameter which is F-measure, Recall, and Precision using the formula stated previously. In the below table we can see the comparisons.

Table 1: Comparison results of F-Measure, Recall, and Precision between Otsu, Niblack, Sauvola and proposed method for sample0_1(1024×1024)

Method	**F- Measure**	**Recall**	**Precision**
Otsu	0.891	0.992	0.808
Niblack	0.868	0.978	0.78
Sauvola (WS = 5)	0.894	0.95	0.844
Sauvola (WS = 7)	0.915	0.965	0.869
Sauvola (WS = 9)	0.933	0.972	0.896
Sauvola (WS = 11)	0.935	0.973	0.9
Sauvola (WS = 13)	0.927	0.992	0.89
Sauvola (WS = 15)	0.919	0.965	0.877
Sauvola (WS = 17)	0.912	0.962	0.866
Sauvola Ensemble (QC ≥ 1)	0.911	0.975	0.855
Sauvola Ensemble (QC ≥2)	0.93	0.978	0.887
Sauvola Ensemble (QC ≥3)	0.947	0.981	0.916
Sauvola Ensemble (QC ≥4)	0.954	0.977	0.933
Sauvola Ensemble (QC ≥5)	**0.956**	0.968	0.945
Sauvola Ensemble (QC ≥ 6)	0.954	0.959	0.95
Sauvola Ensemble (QC ≥7)	0.95	0.946	**0.954**

Where WS means *Selected Window Size,* $QC \geq n$ means *Quality Consensus with at least n window gives the decision.*

5.4.1.2 Second Data sample0_2 (1024×1024)

Similarly, as stated in the first dataset we have again performed the same task and shown the comparison of each method with figures and tables.

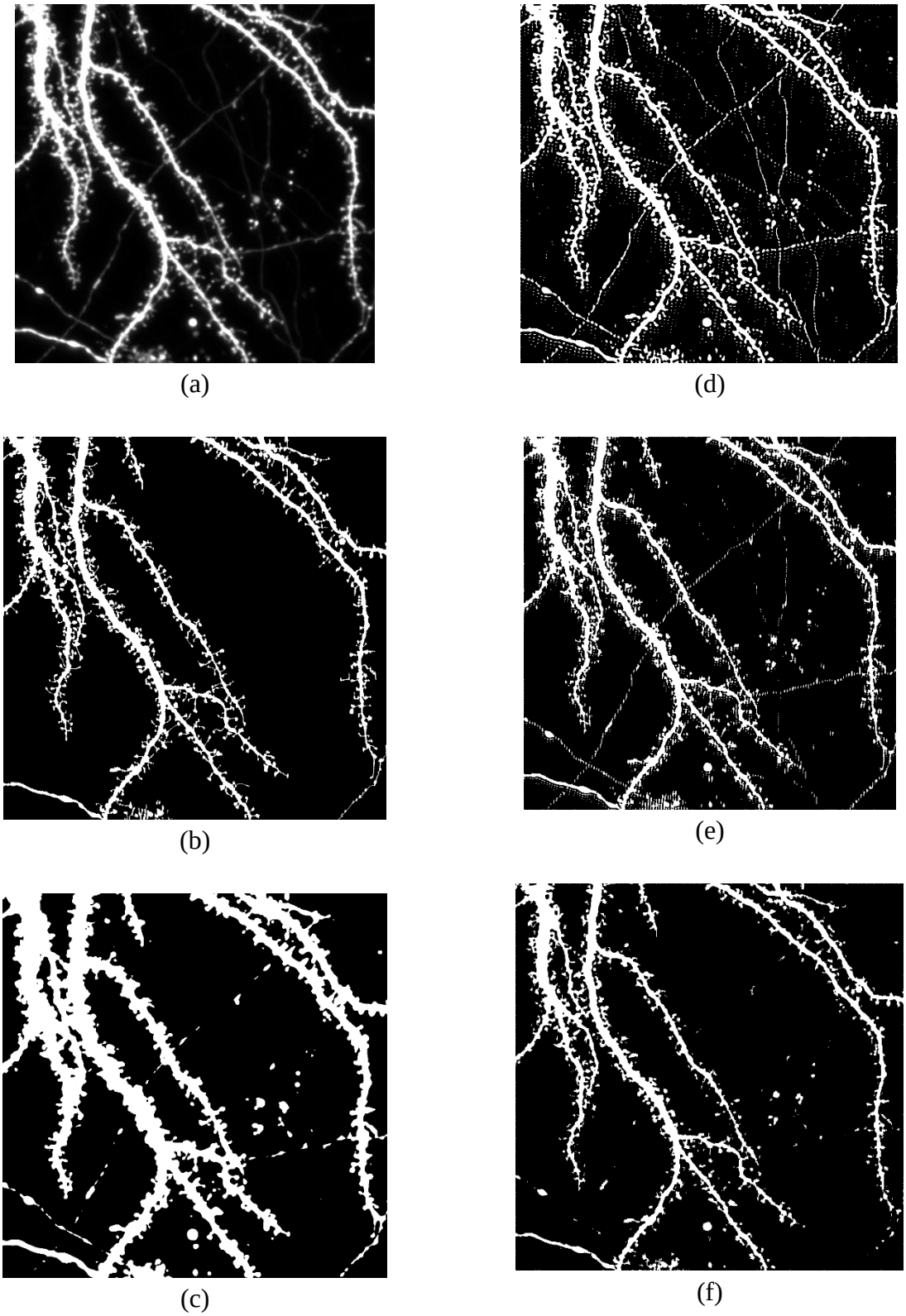

Figure 4: sample0_2 (a) Input Grayscale Image, (b) Prepared Ground Truth, (c) Otsu's Method, (d) Niblack's Method, (e) Sauvola's Method with Window Size =11 (f) Sauvola Ensemble (Quality consensus- at least 7)

Table 2: Comparison results of F-Measure, Recall, and Precision between Otsu, Niblack, Sauvola, and proposed method for sample0_2 (1024×1024)

Method	**F- Measure**	**Recall**	**Precision**
Otsu	0.719	0.989	0.565
Niblack	0.804	0.952	0.695
Sauvola (WS = 5)	0.805	0.864	0.753
Sauvola (WS = 7)	0.821	0.903	0.752
Sauvola (WS = 9)	0.846	0.903	0.796
Sauvola (WS = 11)	0.869	0.931	0.815
Sauvola (WS = 13)	0.863	0.935	0.801
Sauvola (WS = 15)	0.851	0.933	0.782
Sauvola (WS = 17)	0.839	0.93	0.764
Sauvola Ensemble (QC ≥ 1)	0.849	0.928	0.782
Sauvola Ensemble (QC ≥2)	0.86	0.937	0.794
Sauvola Ensemble (QC ≥3)	0.89	0.94	0.845
Sauvola Ensemble (QC ≥4)	**0.906**	0.939	0.875
Sauvola Ensemble (QC ≥5)	0.904	0.918	0.89
Sauvola Ensemble (QC ≥ 6)	0.89	0.896	0.884
Sauvola Ensemble (QC ≥7)	0.875	0.853	**0.898**

Where WS means Selected Window Size, $QC \geq n$ means Quality Consensus with at least n window gives the decision.

5.4.1.3 Third Data sample10_3 (1024×1024)

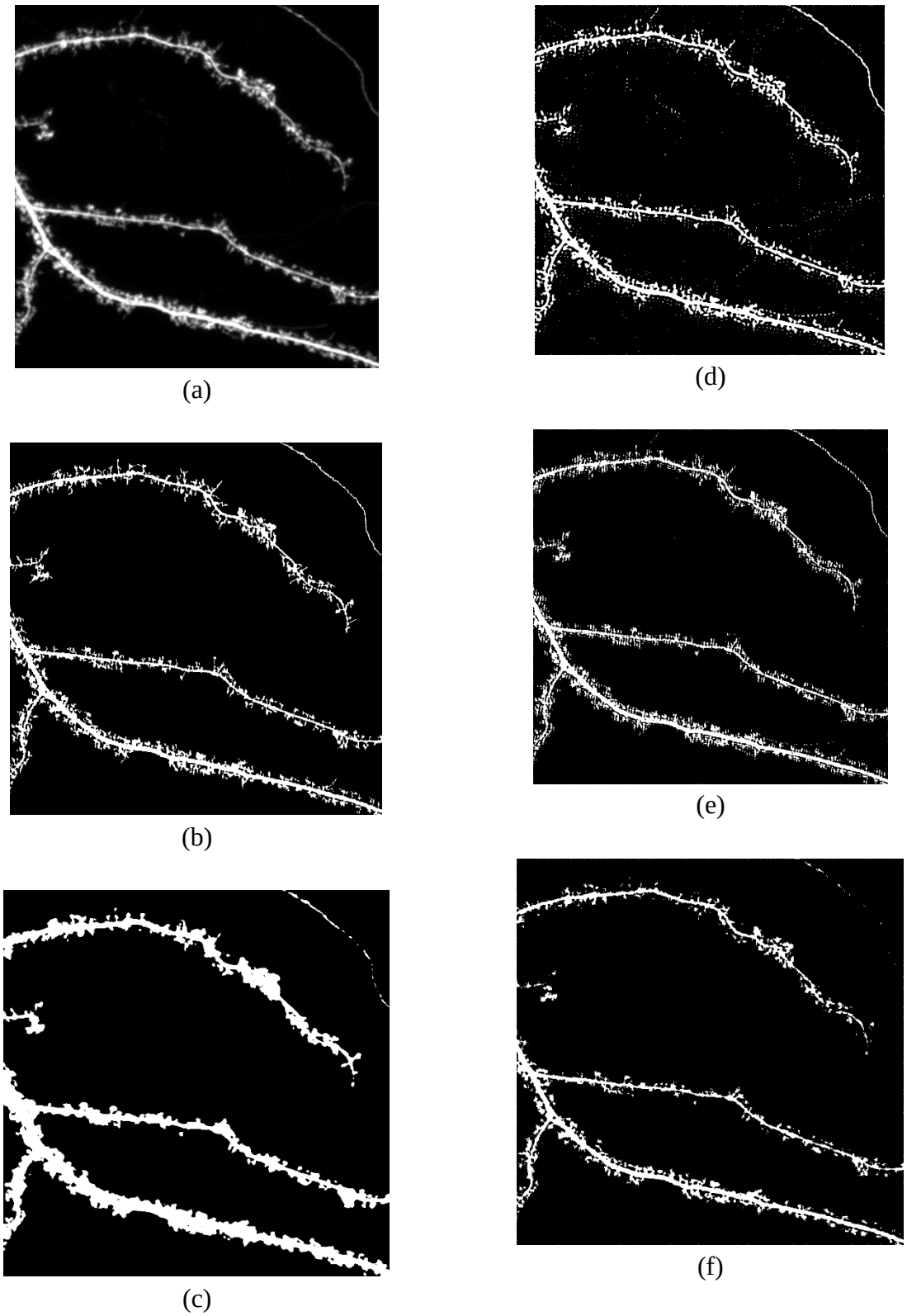

Figure 5:sample10_3 (a) Input Grayscale Image, (b) Prepared Ground Truth, (c) Otsu's Method, (d) Niblack's Method, (e) Sauvola's Method with Window Size =11 (f) Sauvola Ensemble (Quality consensus- at least 7)

Table 3: Comparison results of F-Measure, Recall, and Precision between Otsu, Niblack, Sauvola, and proposed method for sample10_3(1024X1024)

Method	**F- Measure**	**Recall**	**Precision**
Otsu	0.751	0.95	0.621
Niblack	0.829	0.907	0.763
Sauvola (WS =5)	0.756	0.76	0.752
Sauvola (WS =7)	0.792	0.837	0.751
Sauvola (WS =9)	0.819	0.829	0.809
Sauvola (WS =11)	0.886	0.892	0.881
Sauvola (WS =13)	0.879	0.888	0.871
Sauvola (WS =15)	0.865	0.879	0.851
Sauvola (WS =17)	0.851	0.871	0.831
Sauvola Ensemble (QC ≥ 1)	0.821	0.893	0.76
Sauvola Ensemble (QC ≥ 2)	0.857	0.902	0.817
Sauvola Ensemble (QC ≥ 3)	0.899	0.909	0.89
Sauvola Ensemble (QC ≥ 4)	**0.978**	0.965	**0.991**
Sauvola Ensemble (QC ≥ 5)	0.889	0.86	0.919
Sauvola Ensemble (QC ≥ 6)	0.856	0.815	0.901
Sauvola Ensemble (QC ≥ 7)	0.816	0.737	0.915

Where WS means Selected Window Size, $QC \geq n$ means Quality Consensus with at least n window gives the decision.

5.4.4 Forth Data sample1_4 (508×512)

Similarly, we do the same for 508X512 images (Fig: 4(a)) collected as mentioned in the data description chapter previously. Then we apply Otsu's method, Niblack's method, and Sauvola's method (Here in the figure we have shown a window size of 11 but for the experiment we have taken windows of variable sizes ranging from 5 to 17, the result is shown in the below table) and our proposed algorithm (Here in the figure we have shown quality consensus for at least 7 pixels but for the experiment, we have shown all consensus data) on the same image respectively.

In the proposed algorithm we have also applied the noise filter to get rid of unwanted lone white pixels from the output image.

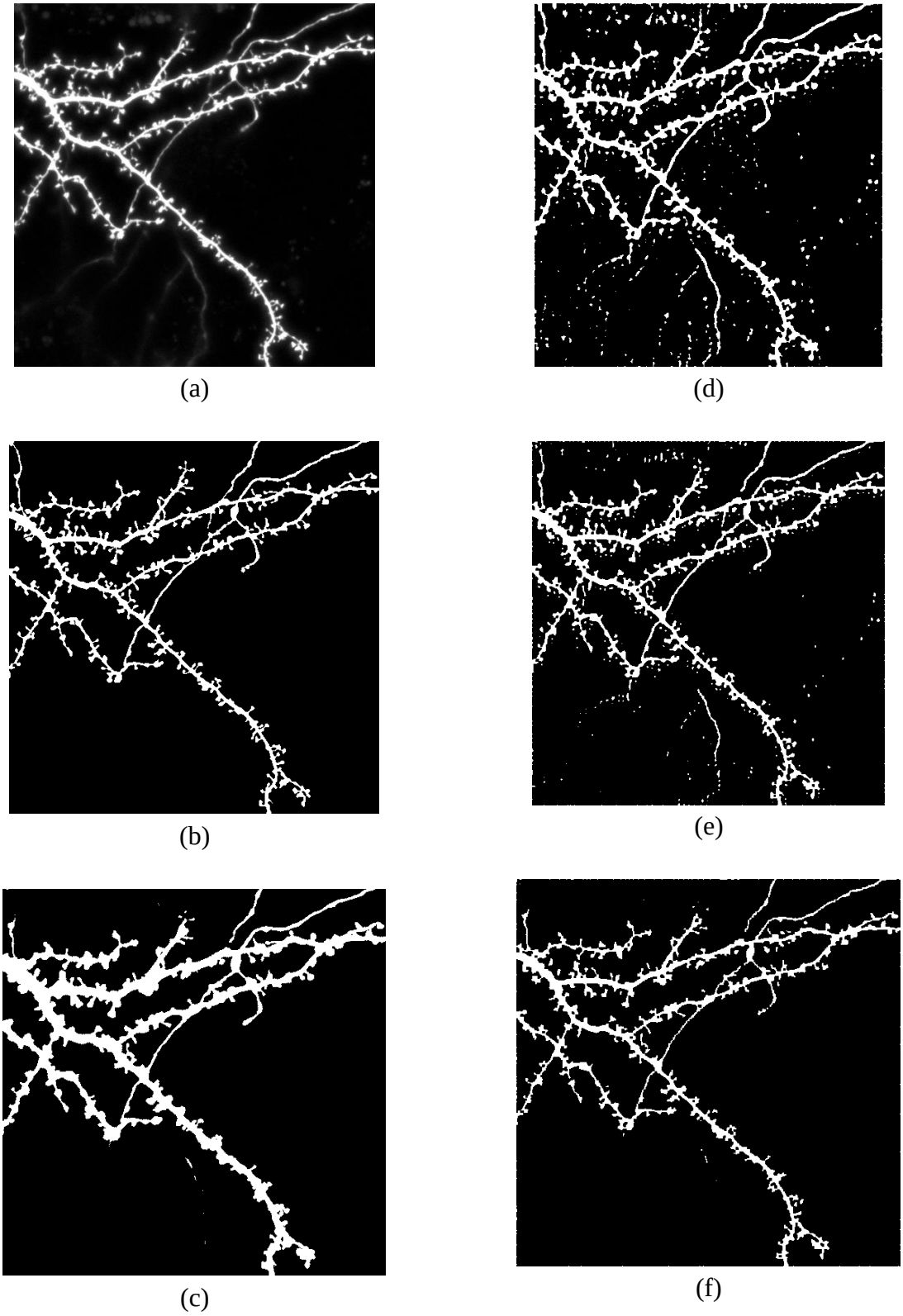

Figure 6:sample1_4 (a) Input Grayscale Image, (b) Prepared Ground Truth, (c) Otsu's Method, (d) Niblack's Method, (e) Sauvola's Method with Window Size =11 (f) Sauvola Ensemble (Quality consensus- at least 7)

After storing all the outputs, we calculated the quality comparison parameter which is F-measure, Recall, and Precision using the formula stated previously. In the below table we can see the comparisons.

Table 4: Comparison results of F-Measure, Recall, and Precision between Otsu, Niblack, Sauvola, and proposed method for sample1_4 (508X512)

Method	**F- Measure**	**Recall**	**Precision**
Otsu	0.801	0.976	0.679
Niblack	0.810	0.982	0.69
Sauvola (WS =5)	0.852	0.968	0.761
Sauvola (WS =7)	0.896	0.918	0.874
Sauvola (WS =9)	0.908	0.952	0.867
Sauvola (WS =11)	0.903	0.965	0.849
Sauvola (WS =13)	0.886	0.97	0.815
Sauvola (WS =15)	0.87	0.97	0.789
Sauvola (WS =17)	0.852	0.968	0.761
Sauvola Ensemble (QC ≥ 1)	0.872	0.969	0.793
Sauvola Ensemble (QC ≥ 2)	0.891	0.976	0.819
Sauvola Ensemble (QC ≥ 3)	0.903	0.975	0.841
Sauvola Ensemble (QC ≥ 4)	0.92	0.968	0.876
Sauvola Ensemble (QC ≥ 5)	**0.93**	0.952	0.908
Sauvola Ensemble (QC ≥ 6)	0.924	0.919	0.929
Sauvola Ensemble (QC ≥ 7)	0.912	0.878	**0.948**

Where WS means Selected Window Size, $QC \geq n$ means Quality Consensus with at least n window gives the decision.

5.4.5 Fifth Data sample7_1 (508×512)

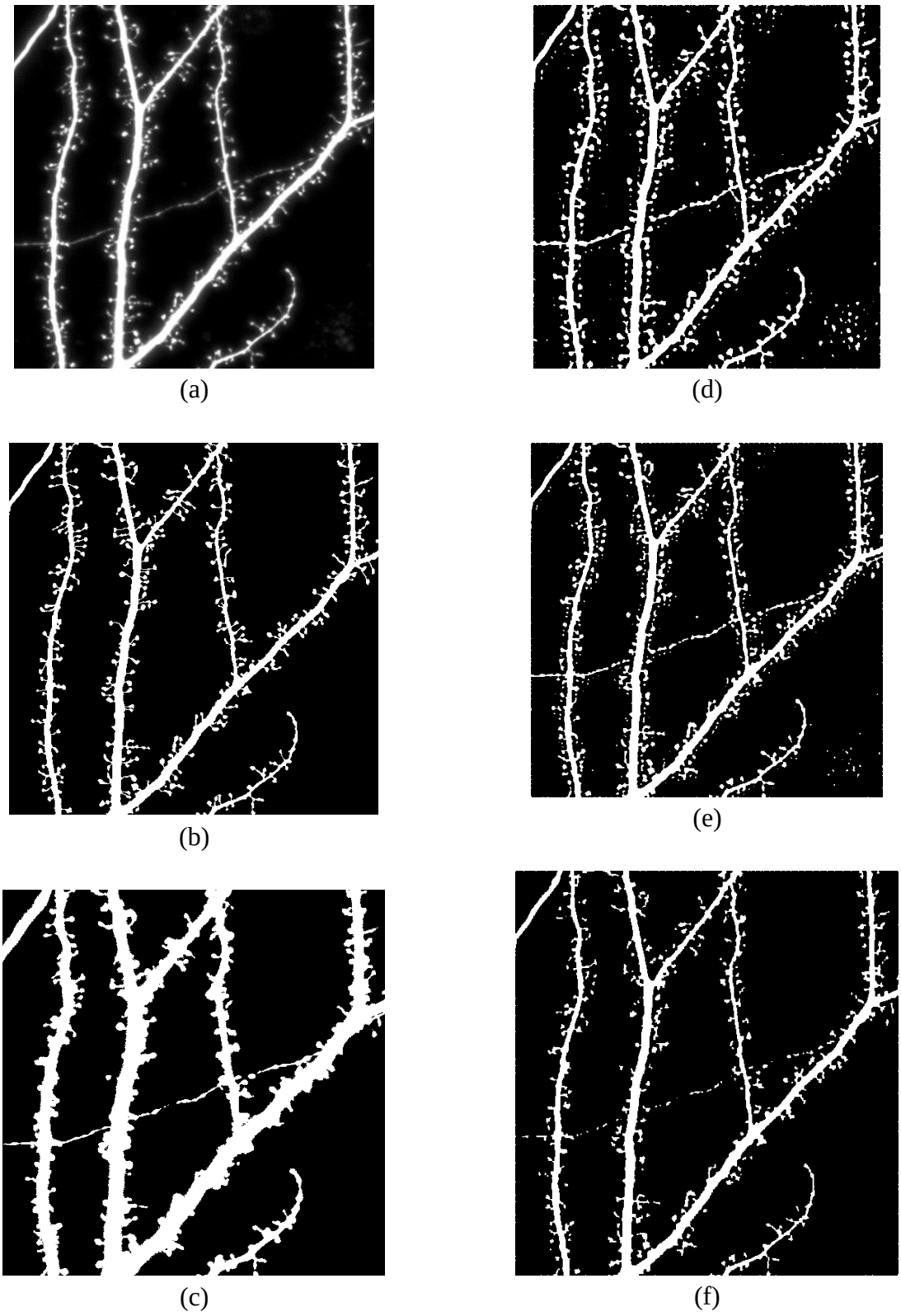

Figure 7:sample7_1 (a) Input Grayscale Image, (b) Prepared Ground Truth, (c) Otsu's Method, (d) Niblack's Method, (e) Sauvola's Method with Window Size =11 (f) Sauvola Ensemble (Quality consensus- at least 7)

Table 5: Comparison results of F-Measure, Recall, and Precision between Otsu, Niblack, Sauvola, and proposed method for sample7_1(508X512)

Method	**F- Measure**	**Recall**	**Precision**
Otsu	0.726	0.989	0.574
Niblack	0.838	0.956	0.746
Sauvola (WS =5)	0.865	0.868	0.863
Sauvola (WS =7)	0.882	0.91	0.855
Sauvola (WS =9)	0.899	0.936	0.865
Sauvola (WS =11)	0.902	0.949	0.858
Sauvola (WS =13)	0.89	0.947	0.839
Sauvola (WS =15)	0.877	0.943	0.82
Sauvola (WS =17)	0.866	0.939	0.804
Sauvola Ensemble (QC ≥ 1)	0.875	0.951	0.809
Sauvola Ensemble (QC ≥ 2)	0.894	0.956	0.84
Sauvola Ensemble (QC ≥ 3)	0.909	0.955	0.867
Sauvola Ensemble (QC ≥ 4)	0.92	0.949	0.893
Sauvola Ensemble (QC ≥ 5)	**0.924**	0.933	0.914
Sauvola Ensemble (QC ≥ 6)	0.917	0.905	0.929
Sauvola Ensemble (QC ≥ 7)	0.905	0.867	**0.946**

Where WS means Selected Window Size, QC≥n means Quality Consensus with at least n window gives the decision.

Here we are including the table of average measurements of F-measure, Recall, and Precision of the above-mentioned five data set images based on the following methods:

Table 6: Comparison results of average F-measure, Recall, and Precision between Otsu, Niblack, Sauvola, and proposed method for taking five datasets

Method	**F- Measure**	**Recall**	**Precision**
Otsu	0.778	0.979	0.649
Niblack	0.829	0.955	0.735
Sauvola (WS = 11)	0.899	0.942	0.861
Sauvola Ensemble (QC ≥5)	**0.921**	0.926	0.915
Sauvola Ensemble (QC ≥7)	0.892	0.856	**0.932**

After calculating the F-measure, recall, and precision it is obvious that the proposed method is giving more accurate results than Otsu's method, Niblack's method, and Sauvola's method. In our proposed algorithm we can see that quality consensus with at least 5 windows having the same decision value provides better F-measure than other algorithms and we can also see that the precision for the output images generated through the proposed method from the comparison that at least 7 windows with the same decision provide better precision. Also by using this method, the shape of the actual image is being preserved quite well.

Despite getting a good f-measure and better precision, our proposed method can't give the output images where all the spine and dendritic mushrooms are connected. After observing it is clear that there exist a few spines that are not connected to the dendrite. Also, our proposed algorithm and implemented python code are time-consuming i.e., the time complexity is a bit high. These methods are often slow since the computation of image features from the local neighbourhood is to be done for each image pixel[15].

CHAPTER 6: CONCLUSION

This thesis introduces an improved version of Sauvola's method suitable for binarizing neuronal and dendritic images. Our proposed method is completely automated from reading the grayscale image to storing the output image.

Here we are selecting the window starting from 5×5 to 17×17 for local thresholding and then decide whether the pixel is going to be white or black according to the quality consensus starting from at least 1 window to all the 7 windows. After binarizing through the proposed method, we have seen that the precision of the output images is increasing depending on how many windows we are going to be considered as shown in the previous chapter. Also, the overall quality and shape of the images are kept intact as shown in the (Fig:7).

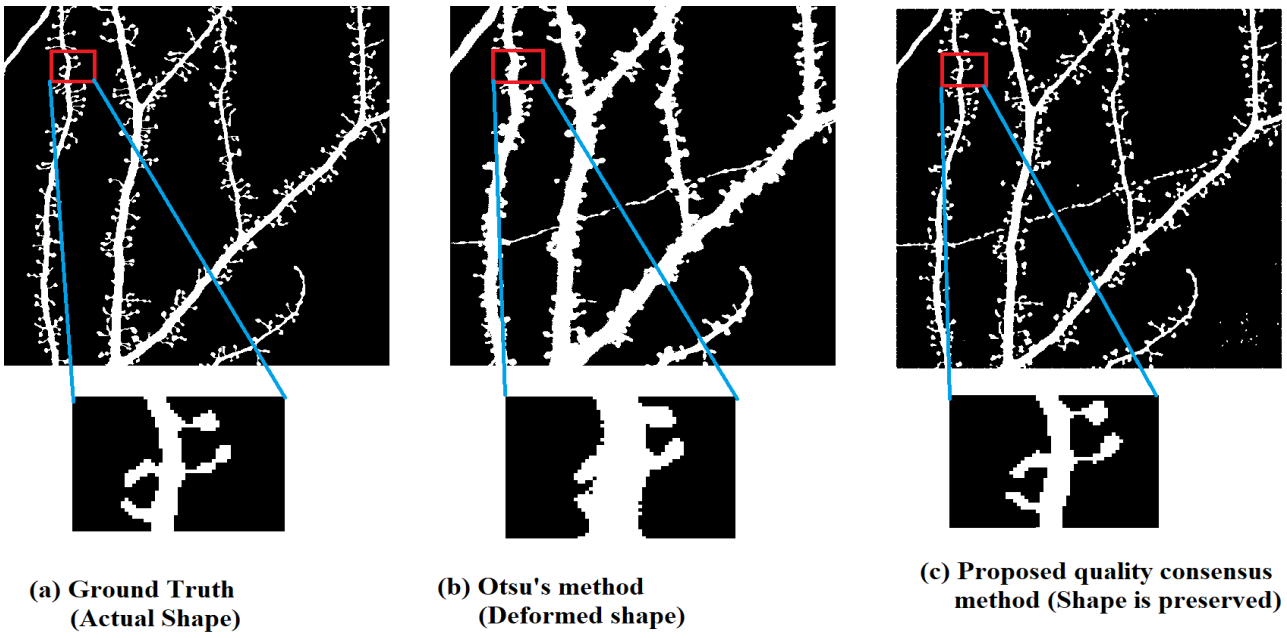

Figure 8: Comparison of a grayscale image, ground truth image, and different output of that particular image for analysing the shape intact quality of the proposed method

Besides these, after applying the morphological close operation on a 3×3 neighbourhood we have seen that a lot of disconnected spine's necks get connected to the dendrite. Here (Fig:8) we are including such an output image's detailed view.

Although we are getting an overall good result, there are still exist a few disconnected spines which can't be joined (Fig: 9) to the dendrite by using a higher neighbourhood considering a morphological closing operation. Besides these, we have prepared only 10 ground truth images because we don't have enough resources.

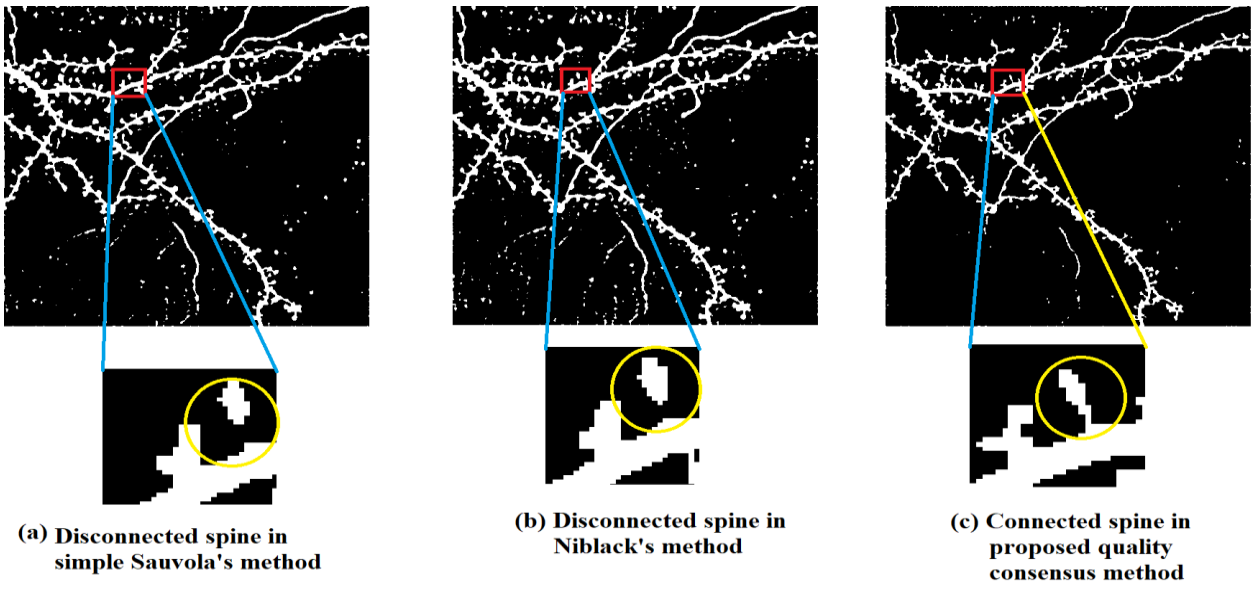

Figure 9: Connected Spines with the dendrite after binarization and closing operation of this image by our proposed method.

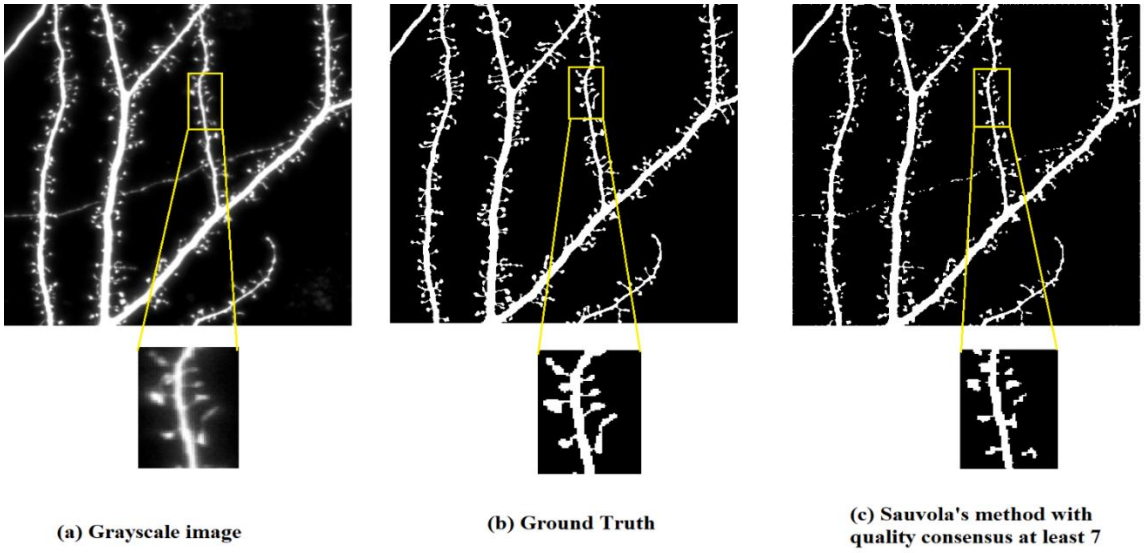

Figure 10:Disconnected Spines from the dendrite after binarization of this image by our proposed method.

By altering the process of choosing the window from the images, this work can be expanded in the future. We can choose the window using quality consensus after using hierarchical quad-tree partitioning, quin tree partitioning, and C.G.-based partitioning. Along with this, the loops utilised here can be examined to reduce the temporal complexity of the implemented Python code and increase performance. Additionally, more real-world data can be collected for better comparisons that would aid in evaluating the suggested approach.

REFERENCES

[1] N. R. Pal and S. K. Pal, "A Review on Image Segmentation Techniques," *Pattern Recognition*, vol. 26, no. 9, pp. 1277–1294, 1993.

[2] R. Rodríguez, "Binarization of medical images based on the recursive application of mean shift filtering : Another algorithm," *Advances and Applications in Bioinformatics and Chemistry*, p. 1, 2008.

[3] T. Sund and K. Eilertsen, "An algorithm for fast adaptive image binarization with applications in radiotherapy imaging," *IEEE Transactions on Medical Imaging*, vol. 22, no. 1, pp. 22–28, Jan. 2003, doi: 10.1109/TMI.2002.806431.

[4] S. Saleh Al-amri and N. Kalyankar, "Image Segmentation by Using Thershold Techniques," *Journal of Computing*, vol. 2, no. 5, pp. 83–86, 2010.

[5] S. Mukhopadhyay and B. Chanda, "Multiscale morphological segmentation of gray-scale images," *IEEE Transactions on Image Processing*, vol. 12, no. 5, pp. 533–549, May 2003, doi: 10.1109/TIP.2003.810757.

[6] K. Somasundaram and P. Kalavathi, "Medical Image Binarization Using Square Wave Representation," *ICLICC, Springer*, vol. 140, pp. 152–158, 2011.

[7] E. H. A and R. N, "OCR Accuracy Improvement on Document Images Through a Novel Pre-Processing Approach," *Signal & Image Processing : An International Journal*, vol. 6, no. 4, pp. 01–18, Aug. 2015, doi: 10.5121/sipij.2015.6401.

[8] R. C. Gonzalez, R. E. Woods, J. Partridge, and J. Bai, *Digital Image Processing*, 2nd ed. Beijing: Publishing House of Electronics Industry, 2007. [Online]. Available: www.pearsoned.com/

[9] K. Somasundaram and P. Kalavathi, "Medical Image Binarization Using Square Wave Representation," 2011.

[10] S. Chauhan, E. Sharma, and A. Doegar, "Binarization Techniques for Degraded Document Images-A Review," *IEEE*, pp. 163–166, 2016.

[11] B. Su, S. Lu, and C. L. Tan, "Robust document image binarization technique for degraded document images," *IEEE Transactions on Image Processing*, vol. 22, no. 4, pp. 1408–1417, 2013, doi: 10.1109/TIP.2012.2231089.

[12] F. Wang, L.-Y. Hou, and H. Huang, "Degraded Chinese rubbing images thresholding based on local first-order statistics," *Second International Workshop on Pattern Recognition*, vol. 10443, pp. 1044307 & #x2F;1-1044307 & #x2F;6, 2017, doi: 10.1117/12.2280301.

[13] T. Taxt, P. J. Flynn, and A. K. Jain, “Segmentation of Document Images,” *IEEE Transactions on Pattern Analysis and Machine Intelligence*, vol. 11, no. 12, pp. 1322–1329, 1989, doi: 10.1109/34.41371.

[14] C. te Lin, J. H. Wang, C. S. Tseng, S. C. Tsai, C. W. Lin, and R. J. Huang, “Improved Binarization Using Morphology-driven Image Resizing and Decomposition,” *2019 IEEE 11th International Workshop on Computational Intelligence and Applications, IWCIA 2019 - Proceedings*, pp. 27–33, Nov. 2019, doi: 10.1109/IWCIA47330.2019.8955018.

[15] B. M. Singh and Mridula, “Efficient binarization technique for severely degraded document images,” *CSI Transactions on ICT*, vol. 2, no. 3, pp. 153–161, Nov. 2014, doi: 10.1007/s40012-014-0045-5.

[16] S. D. Yanowitz and A. M. Bruckstein, “A new method for image segmentation,” *9th International Conference on Pattern Recognition*, pp. 270–275, 1988, doi: 10.1109/ICPR.1988.28220.

[17] Y. Nakagawa and A. Rosenfeld, “Some experiments on variable thresholding,” *Pattern Recognition*, vol. 11, no. 3, pp. 191–204, Jan. 1979, doi: 10.1016/0031-3203(79)90006-2.

[18] C. K. Chow and T. Kaneko, “Automatic boundary detection of the left ventricle from cineangiograms,” *Computers and Biomedical Research*, vol. 5, no. 4, pp. 388–410, Aug. 1972, doi: 10.1016/0010-4809(72)90070-5.

[19] X. Glaw, K. Inder, A. Kable, and M. Hazelton, “Visual Methodologies in Qualitative Research: Autophotography and Photo Elicitation Applied to Mental Health Research,” *International Journal of Qualitative Method*, vol. 16, pp. 1–8, 2017, doi: 10.1177/1609406917748215.

[20] R. Rodríguez, P. J. Castillo, V. Guerra, A. G. Suárez, and E. Izquierdo, “Two Robust Techniques for Segmentation of Biomedical Images Dos Técnicas Robustas para la Segmentación de Imágenes Biomédicas,” *Computación y Sistemas*, vol. 9, pp. 355–369, 2006.

[21] K. M. Harris and S. B. Kater, “Dendritic spines: Cellular specializations imparting both stability and flexibility to synaptic function,” *Annual Review of Neuroscience*, vol. 17, pp. 341–371, 1994, doi: 10.1146/ANNUREV.NE.17.030194.002013.

[22] M. E. Chicurel and K. M. Harris, “Three-dimensional analysis of the structure and composition of CA3 branched dendritic spines and their synaptic relationships with mossy fiber boutons in the rat hippocampus,” *Journal of Comparative Neurology*, vol. 325, no. 2, pp. 169–182, 1992, doi: 10.1002/CNE.903250204.

[23] K. E. Sorra, K. M. Harris, and K. M. Harris, “Overview on the Structure, Composition, Function, Development, and Plasticity of Hippocampal Dendritic

Spines STRUCTURE OF HIPPOCAMPAL DENDRITIC SPINES," *WILEY-LISS, INC*, vol. 10, no. 5, pp. 501–511, 2000, [Online]. Available: http://synapses.

[24] J. C. Fiala, J. Spacek, and K. M. Harris, "Dendritic Spine Pathology: Cause or Consequence of Neurological Disorders?," *Brain Research Reviews*, vol. 39, pp. 29–54, 2002, [Online]. Available: www.elsevier.com/locate/bres

[25] H. Hering and M. Sheng, "Dendritic Spines: Structure, Dynamics and Regulations," *Nature Reviews, Neuroscience*, pp. 880–888, 2001. [Online]. Available: www.nature.com/reviews/neuro

[26] O. von Bohlen und Halbach, "Structure and function of dendritic spines within the hippocampus," *Annals of Anatomy*, vol. 191, no. 6. pp. 518–531, Nov. 20, 2009. doi: 10.1016/j.aanat.2009.08.006.

[27] K. F. H. Lee, C. Soares, and J.-C. B. Bé¨ıque, "Examining Form and Function of Dendritic Spines," *Neural Plasticity*, vol. 2012, 2012, doi: 10.1155/2012/704103.

[28] M. Matsuzaki, N. Honkura, G. C. R. Ellis-Davies, and H. Kasai, "Structural basis of long-term potentiation in single dendritic spines," *Nature*, vol. 429, no. 6993, pp. 761–766, Jun. 2004, doi: 10.1038/NATURE02617.

[29] P. Caroni, F. Donato, and D. Muller, "Structural plasticity upon learning: Regulation and functions," *Nature Reviews Neuroscience*, vol. 13, no. 7, pp. 478–490, Jul. 2012, doi: 10.1038/NRN3258.

[30] C. Sala and M. Segal, "Dendritic spines: The locus of structural and functional plasticity," *Physiological Reviews*, vol. 94, no. 1, pp. 141–188, Jan. 2014, doi: 10.1152/PHYSREV.00012.2013.

[31] J. C. Fiala, J. Spacek, and K. M. Harris, "Dendritic spine pathology: Cause or consequence of neurological disorders?," *Brain Research Reviews*, vol. 39, no. 1, pp. 29–54, 2002, doi: 10.1016/S0165-0173(02)00158-3.

[32] A. Krzystyniak *et al.*, "Prophylactic ketamine treatment promotes resilience to chronic stress and accelerates recovery: Correlation with changes in synaptic plasticity in the CA3 subregion of the hippocampus," *International Journal of Molecular Sciences*, vol. 20, no. 7, Apr. 2019, doi: 10.3390/ijms20071726.

[33] S. B. Chidambaram *et al.*, "Dendritic spines: Revisiting the physiological role," *Progress in Neuro-Psychopharmacology and Biological Psychiatry*, vol. 92, pp. 161–193, Jun. 2019, doi: 10.1016/J.PNPBP.2019.01.005.

[34] T. L. Spires *et al.*, "Neurobiology of Disease Dendritic Spine Abnormalities in Amyloid Precursor Protein Transgenic Mice Demonstrated by Gene Transfer and Intravital Multiphoton Microscopy," 2005, doi: 10.1523/JNEUROSCI.1879-05.2005.

[35] J. R. Glausier and D. A. Lewis, “Dendritic spine pathology in schizophrenia,” *Neuroscience*, vol. 251, pp. 90–107, Oct. 2013, doi: 10.1016/J.NEUROSCIENCE.2012.04.044.

[36] B. Ruszczycki *et al.*, “Sampling issues in quantitative analysis of dendritic spines morphology,” *BMC Bioinformatics*, vol. 13, no. 1, pp. 1–12, Aug. 2012, doi: 10.1186/1471-2105-13-213/FIGURES/7.

[37] B ̨aczy ́nska Ewa, K. K. Pels, S. Basu, J. Włodarczyk, and Bła ̇Zej Ruszczycki, “Molecular Sciences Quantification of Dendritic Spines Remodeling under Physiological Stimuli and in Pathological Conditions,” *J. Mol. Sci*, p. 22, 2021, doi: 10.3390/ijms22084053.

[38] K. P. Berry and E. Nedivi, “Spine Dynamics: Are They All the Same?,” *Neuron*, vol. 96, no. 1, pp. 43–55, Sep. 2017, doi: 10.1016/J.NEURON.2017.08.008.

[39] D. A. Richards *et al.*, “Glutamate induces the rapid formation of spine head protrusions in hippocampal slice cultures,” *Proc Natl Acad Sci U S A*, vol. 102, no. 17, pp. 6166–6171, Apr. 2005, doi: 10.1073/PNAS.0501881102.

[40] H. Hering and M. Sheng, “Dentritic spines: structure, dynamics and regulation,” *Nature Reviews Neuroscience*, vol. 2, no. 12, pp. 880–888, 2001, doi: 10.1038/35104061.

[41] S. Basu *et al.*, “Quantitative 3-D morphometric analysis of individual dendritic spines,” *Scientific Reports*, vol. 8, no. 1, Dec. 2018, doi: 10.1038/s41598-018-21753-8.

[42] J. Sauvola and M. PietikaKinen, “Adaptive document image binarization,” *Pattern Recognition*, vol. 33, pp. 225–236, 2000.

[43] N. Otsu, “A threshold selection method from gray-level histograms,” *IEEE Trans. Sys. Man. Cyber*, pp. 62–66, 1979.

[44] W. Niblack, “An introduction to digital image processing,” *Prentice Hall, Eaglewood Cliffs*. Prentice Hall, Eaglewood Cliffs, pp. 115–116, 1986.

[45] J. Bernsen, “Dynamic thresholding of gray level images,” in *Proceedings of International Conference on Pattern Recognition (ICPR)*, 1986, pp. 1251–1255.

[46] B. Su, S. Lu, and C. L. Tan, “Binarization of Historical Document Images Using the Local Maximum and Minimum,” *Image (Rochester, N.Y.)*, Association for Computing Machinery, pp. 159–166, 2010.

[47] R. Farrahi Moghaddam and M. Cheriet, “AdOtsu: An adaptive and parameterless generalization of Otsu’s method for document image binarization,” *Pattern Recognition*, vol. 45, no. 6, pp. 2419–2431, Jun. 2012, doi: 10.1016/j.patcog.2011.12.013.

[48] S. Basu *et al.*, “2dSpAn: semiautomated 2-d segmentation, classification and analysis of hippocampal dendritic spine plasticity,” *Bioinformatics, Oxford University Press*, vol. 32, no. 16, pp. 2490–2498, 2016, [Online]. Available: http://bioinformatics.oxfordjournals.org/

[49] J. Schindelin *et al.*, “Fiji: An open-source platform for biological-image analysis,” *Nature Methods*, vol. 9, no. 7. pp. 676–682, Jul. 2012. doi: 10.1038/nmeth.2019.

[50] Y. PA *et al.*, “User-guided 3D active contour segmentation of anatomical structures: significantly improved efficiency and reliability,” *Neuroimage*, vol. 31, no. 3, 2006, doi: 10.1016/J.NEUROIMAGE.2006.01.015.

[51] M. Magnowska *et al.*, “Transient ECM protease activity promotes synaptic plasticity,” *Scientific Reports*, 2016, doi: 10.1038/srep27757.

[52] E. H. Barney Smith, L. Likforman-Sulem, and J. Darbon, “Effect of pre-processing on binarization,” *Document Recognition and Retrieval XVII*, vol. 7534, pp. 75340H-75340H–8, Jan. 2010, doi: 10.1117/12.840606.

[53] F. Wang, L.-Y. Hou, and H. Huang, “Degraded Chinese rubbing images thresholding based on local first-order statistics,” *Second International Workshop on Pattern Recognition*, vol. 10443, pp. 1044307/1-1044307/6, Jun. 2017, doi: 10.1117/12.2280301.

[54] N. R. Pal and D. Bhandari, “On object background classification,” *International Journal of Systems Science*, vol. 23, no. 11, pp. 1903–1920, 1992, doi: 10.1080/00207729208949429.